Anal. Bioanal. Electrochem., Vol. 17, No. 8, 2025, 721-746
https://www.doi.org/10.22034/abec.2025.733516

Analytical & Bioanalytical Electrochemistry

Review

Synthesis, Characterization, and Electrochemical Studies of Ni Complexes

Vivek Sharma,[1,*] Rajasekhar VSR Pullabhotla,[2] Akash Kumar Mishra,[3] and Ankit Mittal[4,*]

[1]*Department of Chemistry, GLA University, Mathura, Uttar Pradesh-281406, India*
[2]*Department of Chemistry, Faculty of Science, Agriculture and Engineering, University of Zululand, P/Bag X1001, KwaDlangezwa, 3886, South Africa*
[3]*Department of Chemistry, University of Lucknow, Lucknow, UP-226007, India*
[4]*Department of Chemistry, Shyam Lal College, University of Delhi, Delhi-110032, India*

*Corresponding Author, Tel.: +919627960002
E-Mails: vivek.sharma@gla.ac.in ; ankitmittal070@gmail.com

Received: 16 July 2025 / Received in revised form: 30 September 2025 / Accepted: 30 October 2025 / Published online: 31 December 2025

Abstract- Nickel-based complexes are increasingly studied due to their promising roles in medicine, catalysis, and energy storage. This review offers an in-depth survey of recent progress in the synthesis of nickel complexes, with emphasis on methods involving both organic and inorganic ligands. The influence of ligand type on the stability, geometry, and electronic characteristics of these complexes is discussed in detail. Key analytical techniques, such as UV-Vis spectroscopy, FTIR, NMR, and X-ray diffraction, are highlighted for their importance in characterizing the structure and composition of nickel complexes. The review also examines the electrochemical properties of these compounds, focusing on their redox behavior and potential applications as catalysts in energy-related processes. Critical factors influencing the performance and reactivity of nickel complexes, including ligand environment, nickel oxidation state, and coordination geometry, are identified and analyzed. This article aims to provide valuable insights for researchers focusing on the design, characterization, and diverse applications of nickel-containing complexes in various scientific fields.

Keywords- Nickel complexes; Electrochemical behavior; Macrocylic ligands; Schiff's base ligands; Tetraazmacrocycles

1. INTRODUCTION

Metal complexes serve a key function in various domains, especially in biological applications, where they function as agents against cancer, inflammation, viral infections, and malaria [1-4]. Their unique properties, such as the ability to facilitate electron transfer and form stable bonds with biomolecules, make them essential in developing novel therapeutic strategies and enhancing drug delivery systems [5-7]. Macrocyclic complexes typically exhibit greater stability compared to acyclic polydentate complexes containing the same donor atoms [8-10]. This enhanced stability is due to the metal ion being securely enclosed within the macrocyclic cavity. Consequently, such complexes generally exhibit increased resistance to degradation, improved thermal stability, and enhanced inertness toward hydrolysis by acids and bases. Additionally, many of these complexes exhibit significant antibacterial and antifungal properties [11-13]. Research demonstrates that the antimicrobial efficacy of metal ions can be enhanced through their combination with diverse ligands [14]. The coordination of metal ions with polydentate ligands has garnered significant interest because of their unique spectral, magnetic, and biological properties [15].

Electrochemical studies of metal complexes have provided valuable information on their redox properties, stability, and prospective uses in catalysis and energy storage [16-18]. Optimizing the electronic properties of metal complexes could lead to enhanced performance in various electrochemical processes, paving the way for more efficient and sustainable energy solutions. Metal complexes with tailored ligands, may further improve their electrochemical characteristics and broaden their applicability in next-generation devices [19]. Research on Schiff base ligands and associated 3d-transition metal complexes has played a key role in the development of organometallic and bioinorganic chemistry [20-22]. Schiff base ligands are particularly noteworthy for their adaptability, which can be further increased by hydrogenating their C=N bonds. This modification enhances their metal-binding ability, which has drawn growing attention to reduced Schiff bases [23-25].

Ni(II) tetrazamacrocyclic complexes have attracted considerable attention because of their wide-ranging applications, especially in catalysis and nanotechnology [26]. Nickel complexes exhibit a range of coordination numbers, influenced by various factors [27]. One key factor is the nature of the ligand's donor atoms, which interact with the metal ion and significantly affect the complex's geometry and stability. The stereochemistry of the complex, which refers to the spatial arrangement of atoms around the metal center, also affects the coordination environment and the reactivity of the complex. Furthermore, the charge and Lewis's acidity of the Ni ion

are key determinants for its ability to coordinate with various ligands and catalyze specific reactions [28].

In addition, Ni complexes have gained attention for their antimicrobial properties, with numerous studies highlighting their potential as effective agents against bacteria, fungi, and other pathogens [29-31]. Ligand type, nickel's oxidation state, and the overall coordination framework play key roles in governing the antimicrobial activity of Ni complexes [32,33].

2. SYNTHESIS OF NI COMPLEXES

The template method for the synthesis of metal complexes is a strategic approach where a central metal ion acts as a structural template to direct the assembly of ligands into a specific geometric arrangement, often resulting in the formation of a desired coordination complex [34]. This method influences the ability of the metal ion to influence ligand orientation and reactivity, particularly in cases where the free ligands might not spontaneously form the desired product. Typically, the metal ion is introduced into a reaction mixture containing potential ligands, guiding their condensation or cyclization to form a stable complex with specific stereochemistry or topology. Template synthesis is widely used in the preparation of macrocyclic ligands, Schiff bases, and other specialized coordination compounds [35].

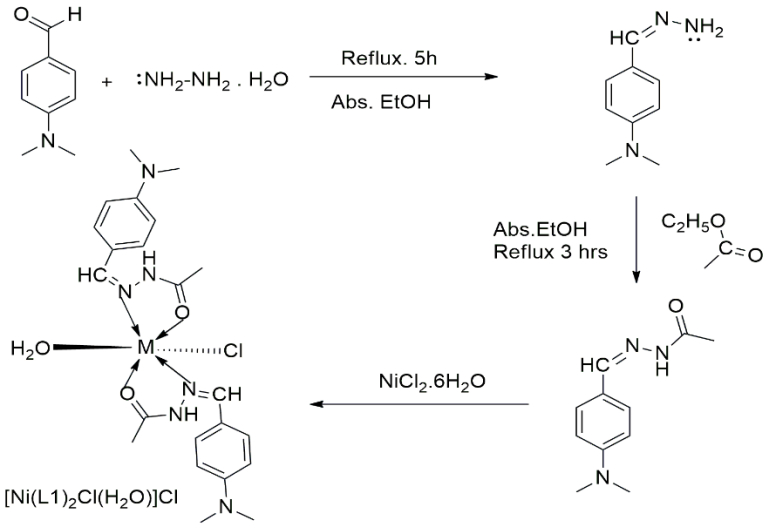

Figure 1. Scheme for the synthesis of $[Ni(L1)_2Cl(H_2O)]Cl$ (Complex **1**)

Recently, Mustafa et al (2024) prepared Ni(II) complex (**1**) using N'-(4-(dimethylamino)benzylidene)acetohydrazide, represented as **L1** [36]. The preparation of the ligand L1 involves two main steps (Figure 1). In the first step, N'-(4-(methanehydrazonoyl)-N,N-dimethylaniline is synthesized by reacting N,N-dimethylaminobenzaldehyde with hydrazine hydrate in ethanol, followed by refluxing for 5 hours. The resulting product is then filtered, washed, and the yield obtained is 85%. In the second step, L1 was prepared by reacting

ethyl acetate with the compound synthesized in step I in an ethanolic medium with a few drops of concentrated HCl. After refluxing for 3 hours, the solvent is evaporated, and the product is filtered, washed, and recrystallized in ethanol to yield ligand L1. Further, the ligand L1 was dissolved in ethanol, followed by the addition of metal salt solution of Ni(II) to the ligand solution in a 2:1 molar ratio. The obtained materials were refluxed and stirred at 80°C for 5 h. After cooling, the product was filtered and sequentially washed with a water-methanol (1:3) solution, followed by petroleum ether. After drying in a vacuum desiccator with anhydrous $CaCl_2$, the complex was recrystallized using methanol [36].

Ogawa et al. (2024) synthesised Ni(II) complex (**2**) using Hexa(1,10-phenanthroline) macrocycle (H_2HAM) as ligand (**L2**) (Figure 2) [37]. Briefly, 0.6432 g (1.66 mmol) H_2HAM (**L2**) and 0.5968 g (1.67 mmol) $Ni(OTf)_2$ was mixed in 15 mL of ethylene glycol in a reaction vessel. The sealed vessel was placed in a microwave synthesis unit, heated to 200°C, and maintained at this temperature for 10 minutes. After reaching room temperature, the solvent was removed by filtration, and the solid residue was washed with acetone. Yellow single crystals of the complex were obtained and dried under reduced pressure.

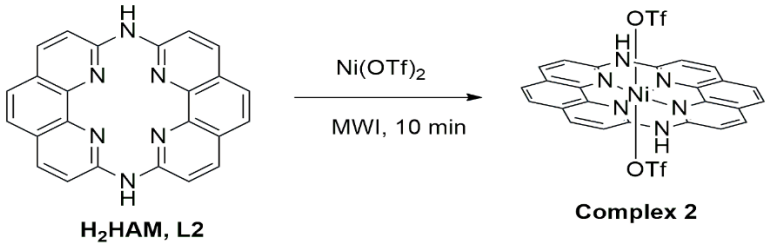

Figure 2. Synthesis of NiN_4 (Complex **2**)

Recently, Vashistha et al. (2024) reported the synthesis of NiN_4 complex (**3**) by involving the template method. Firstly, the ligand **L3** was synthesised by dissolving 2,3-diamino naphthalene (DAN) (0.002 mol) and 2,6-diethyl carboxylate (DEC) (0.002 mol) in methanol (0.002 mol). This templated condensation resulted into Schiff base macrocyclic ligand (**L3**), as shown in Figure 3. This mixture is then treated with methanolic solutions of $NiCl_2 \cdot 6H_2O$ (0.001 mol). The reaction is refluxed for 8 hours, yielding dark brown powder of complex, which are subsequently recrystallized in the mother liquor [38].

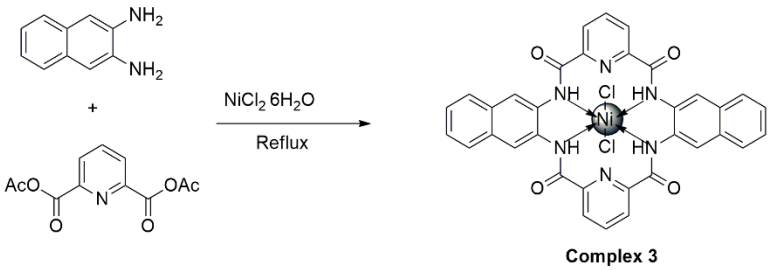

Figure 3. Scheme for the synthesis of complex **3**

Yousri et al. (2024) demonstrated the synthesis of $[Ni(MorphBPT)(H_2O)_3]Cl_2 \cdot 2H_2O$ (Complex **4**) using s-triazine derivatives namely, "2,4-bis(3,5-dimethyl-1H-pyrazol-1-yl)-6-methoxy-1,3,5-triazine" (OMeBPT) as a chelating ligand (**L4**). The complex **4** with the metal ions coordinating display distorted octahedral geometry (Figure 4) [39]. N-thiocarbamoylpyrazolines are versatile polydentate ligands that can be readily synthesized and form stable metal complexes with different geometries. These are the compounds with both thiosemicarbazone and heterocyclic structures, making them significant for pharmacological use. For instance, 1-(N-phenylthiocarbamoyl)-pyrazoline ligands (**L5-L9,** Figure 4) were synthesized from "1-pyridyl-3-aryl-2-propen-1-ones" (1a-e) in moderate yields (32–57%). The preparation of Ni(II) coordination compounds (**4-8**) was achieved using a two-phase solvent system [40].

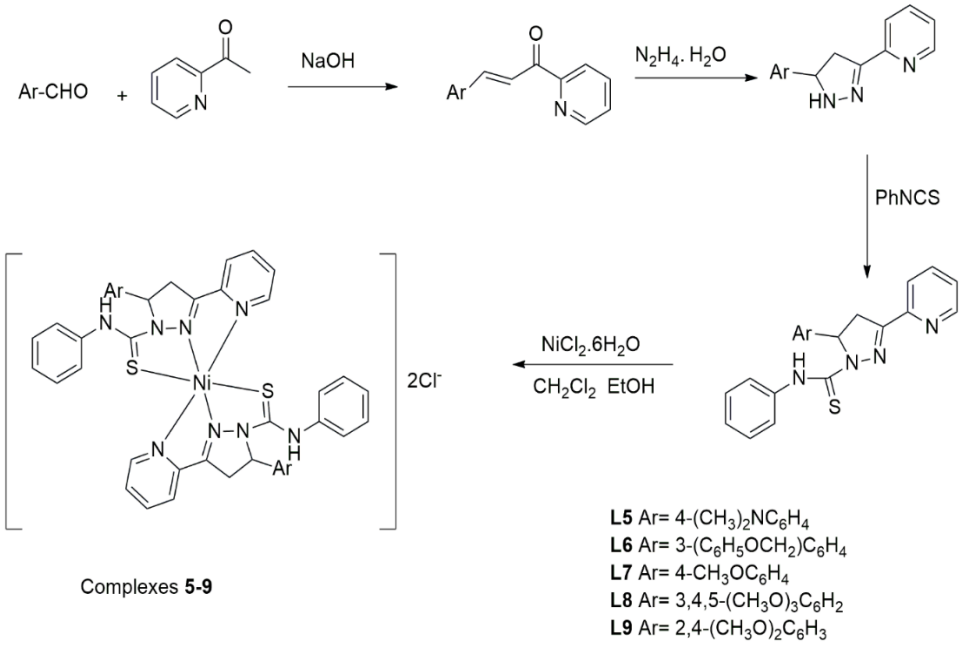

Figure 4. Scheme for the synthesis of Ni complexes (**5-9)** with 1-(N-phenylthiocarbamoyl)-pyrazoline ligands (**L5-L9)**

Remiya et al. (2023) described the synthesis of $[Ni(C_{11}H_{22}N_4)Cl_2]$ (complex **10**) using a condensation reaction between pentane-1,5-dial and triethylenetetramine in the presence of Ni(II) salts in a methanolic solution. This process produced mononuclear 15-membered tetraazamacrocyclic Schiff base complex **10** with the formula $[Ni(C_{11}H_{22}N_4)Cl_2]$ [41]. Further, Babu and co-workers (2023) prepared the Schiff base ligand (**L11**) by stirring 5-cyclohexyl-2-methoxyaniline and salicylaldehyde in equal molar quantities (10 mM each) in methanol and heated to 60–65 °C (Figure 5). After six hours of reflux with stirring, the reaction progress was checked by TLC, and the product was subsequently dried under vacuum using anhydrous $CaCl_2$. Further to synthesize the Ni complex (**11**), the Schiff base (20 mM) was mixed with

nickel acetate salts (10 mM) in hot methanol. The reaction mixture was refluxed at 60–70°C for seven hours, after which the solid products were collected by filtration, washed with hot methanol and petroleum ether, and dried under vacuum over anhydrous $CaCl_2$ [42].

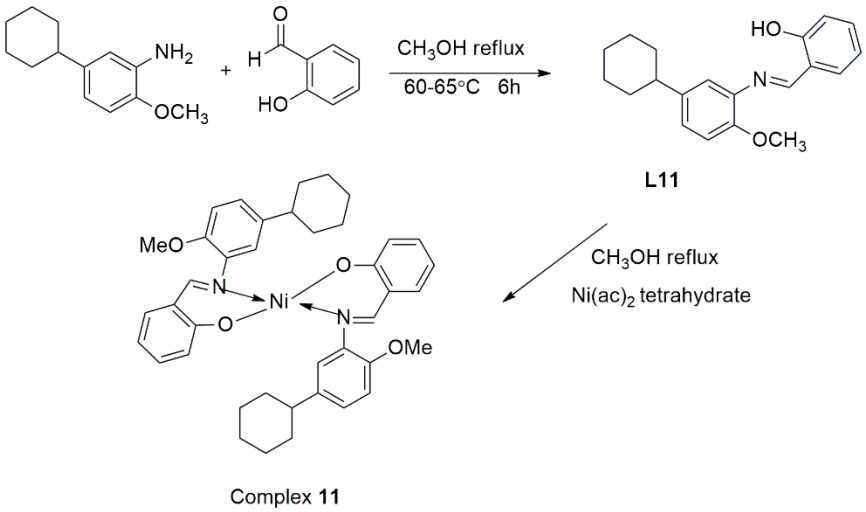

Figure 5. Scheme for the synthesis of Ni(II) complex **11**

Wang and colleagues (2023) synthesised a series of Ni(II) complexes (**12-21,** Figure 6) by reacting $NiCl_2$ with ten different "4′-(4-phenyl)-2′,2′:6′,2″-terpyridine ligands" labelled as **L12-L21**. The reaction resulted in sandwich-like coordination compounds [43].

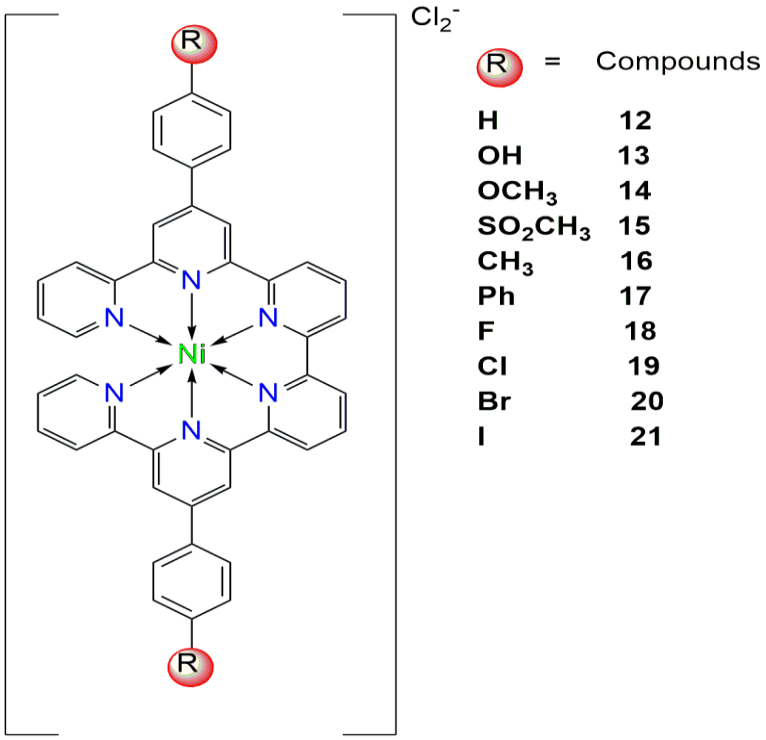

Figure 6. Structures of Ni (II) complexes (**12-21**)

Ravinder et al. (2022) demonstrated the synthesis of Ni-N_4 complex (**22**) using template method. Briefly, 0.216 g (2 mol) of 2,3-diaminobenzene and 0.446 g (2 mol) of "2,6-pyridinecarboxylic acid diethyl", were mixed in methanol to get the ligand (**L22)**, which further treated with 0.162 g (1 mol) of Ni(II) chloride to achieve complex **22** as final product (Figure 7). The content was refluxed for 6 h to get a black powdery material. Afterward, the mixture is concentrated using a rotary evaporator and dried in a desiccator. To yield macrocyclic complex **22**, the crystals were dissolved in an ethanol–ether mixture (1:1) and subjected to recrystallization [44].

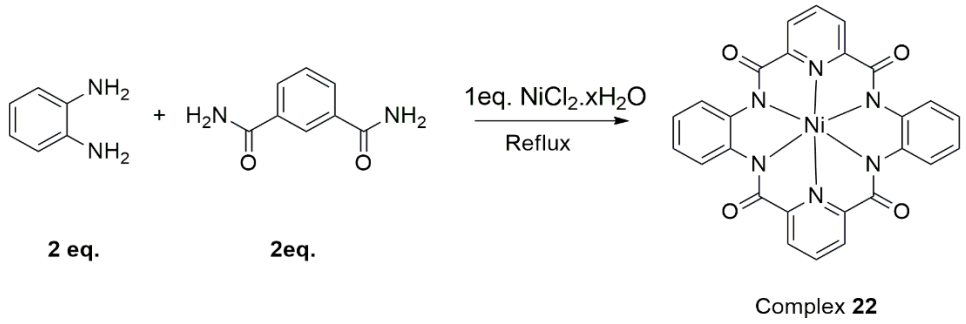

Figure 7. Scheme for the synthesis of Ni (II) complex (**22**)

In the recent past, Vashistha & group (2023) synthesised two Ni macrocyclic complexes (**23, 24)**. First complex (**23**) was synthesized by refluxing a mixture of 3,5-diaminobenzoic acid (2 mol), 1,3-diacetyl (2 mol), and $NiCl_2$ (1 mol) in methanol for six hours. The reaction mixture was then treated with a few drops of $HClO_4$ and permitted to cool to room temperature, yielding light green powder of complex **23**, which were purified using methanol. Similarly, a second complex **(24)** was prepared using o-phenylenediamine and a different ratio of 1,3-diacetyl, following the same procedure (Figure 8) [45].

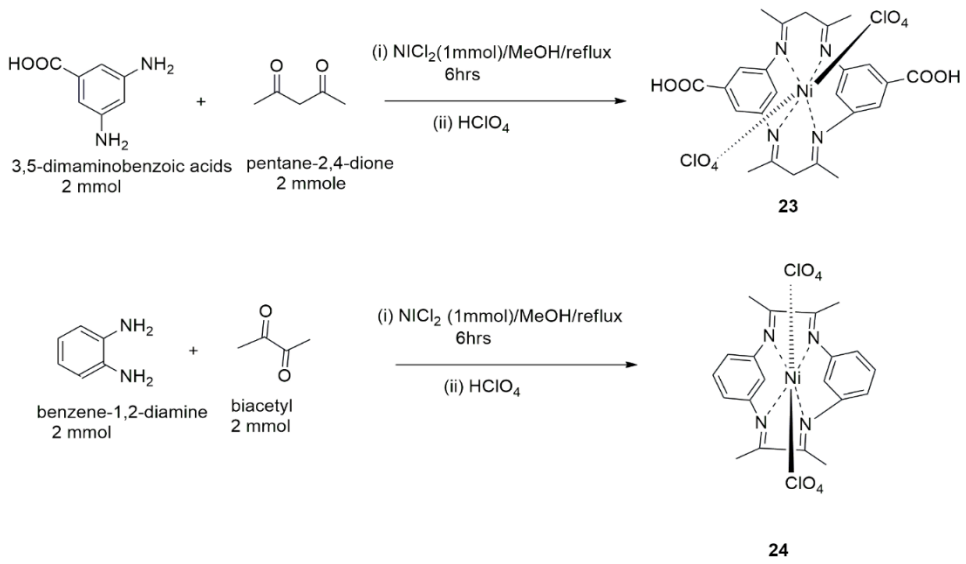

Figure 8. Scheme for the synthesis of two Ni complexes **23** & **24**

Polyazamacrocyclic compounds are a prominent class of macrocyclic complexes. These compounds can be synthesized through a condensation reaction between amines and carbonyl compounds, using suitable matrices. For instance, Ni complexes (**25)** with fully conjugated 14-membered hexaaza ligand (**L25**) were prepared using template cyclo-condensation reactions by Lozovan & group (2025). These involved 2,6-diacetylpyridine and 2,6-pyridinedicarbohydrazide or hydrazine in the presence of Ni(II) ions as directing metal cations. The resulting macrocyclic ligands, coordinated through four nitrogen atoms, formed planar structures with fused metallocycles, including two five-membered and two six-membered chelates. The synthesis typically began with the preparation of soluble nitrate complexes, followed by crystallization. Refluxing the ligand in vinyl cyanide for 12 hours produced monocrystalline forms, which were filtered and evaporated after cooling [46].

The preparation of NiN_4 macrocyclic complex, (Complex **26)**, Figure 9, involves using the ligand "dichloro-[2,4,9,13,15,20-hexamethyldibenzo-1,4,8,11-tetraazacyclotetradecatetraene, **L26**]". The synthesis process typically begins by reacting the metal salts (Ni) with the ligand in an appropriate solvent. The reaction mixture is then heated and stirred under controlled conditions to promote complex formation. Following the reaction, the product is isolated, purified, and characterized to confirm the formation of the desired macrocyclic complex **26** [47].

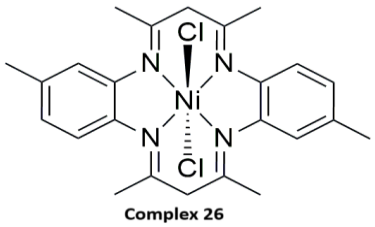

Figure 9. Structure of Ni complex **26**

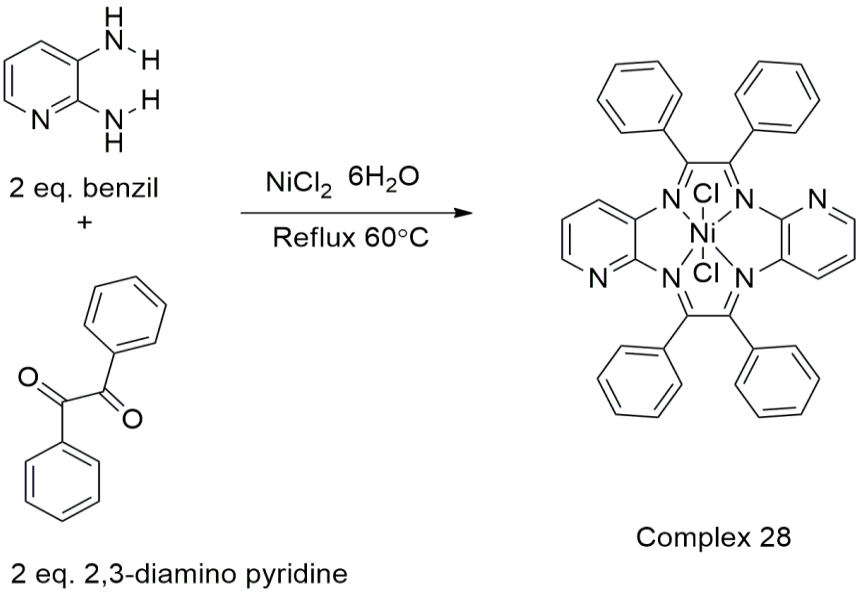

Figure 10. Scheme for the synthesis of Ni complex **28**

A novel tetra-azamacrocyclic ligand ($C_{24}H_{16}N_{12}O_2S_4$), L**27**) and its metal complex, [$NiLCl_2$] (**27**) was synthesised. Analytical data and spectroscopic studies verified that the Ni(II) complex adopts an octahedral geometry [48]. The preparation of the macrocyclic complex [$Ni(L)Cl_2$] (**28,** Figure 10) involves combining 2,3-aminopyridine (DAPy, 2 mol) and benzyl (2 mol) with $NiCl_2.6H_2O$ (1 mol) in 30 mL of methanol using a round-bottom flask. The reaction mixture was refluxed at 60 °C for 6–8 hours. Afterward, the solution is concentrated and then dried using a rotary evaporator. Upon cooling to room temperature, crystals of dark brown colour form, which are washed with a methanol-acetone mixture and then recrystallized in methanol [49].

Shebl et al. (2020) synthesized a mononuclear Ni(II) complex (**29**) using a hydrazone ligand (**L29**) derived from "2-cyano-N′-((4-oxo-4H-chromen-3-yl)methylene)acetohydrazide". The investigation showed that the hydrazone ligand fumctions as a monoanionic tridentate donor, coordinating via γ-pyrone oxygen, enolic oxygen, and azomethine nitrogen atoms. The synthesized metal complexes exhibited neutral mononuclear forms with different stoichiometries (1:1 and 1:2) and ternary complexes (1:1:1) [50]. The preparation of NiN_4 Schiff's base tetraazamacrocyclic complex (**30,** Figure 11) involves reacting triethylenetetraamine, 2,6-diacetyl pyridine, and $NiCl_2.6H_2O$ in methanol. The mixture is refluxed for 6-8 hours, producing a dark brown solution. The product is then concentrated using a rotary evaporator and left in a desiccator overnight to form dark brown coloured crystals of the Ni(II) complex **30**, which are further recrystallized [51].

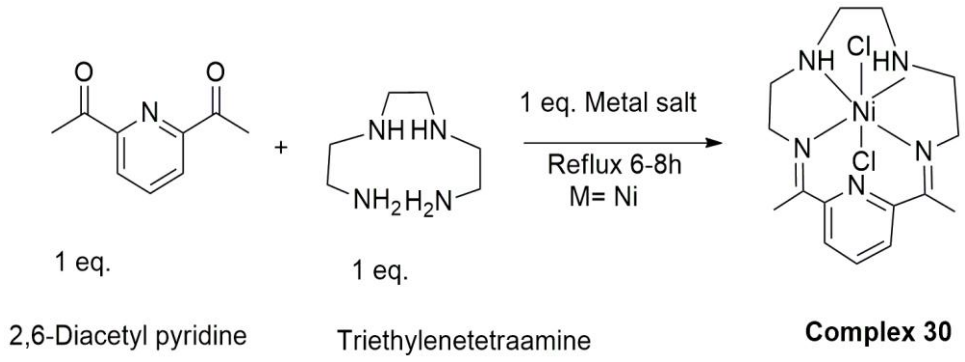

Figure 11. Synthetic scheme of Ni(II) complex **30**

The Ni(II) complex (**31**) is synthesized by mixing 2 moles of '2,3-diamino toluene" (2,3-DAT) and 2 moles of acetylacetone (AA) in 10 mL methanol, with constant stirring. To this solution, 1 mole of $NiCl_2.6H_2O$ is added (Figure 12). The mixture is then refluxed for 6 hours at 60ºC until a dark brown solution forms. The mixture is concentrated using a rotary evaporator, placed in a desiccator overnight, and recrystallized in methanol, yielding the brown-colored Ni(II) complex [52].

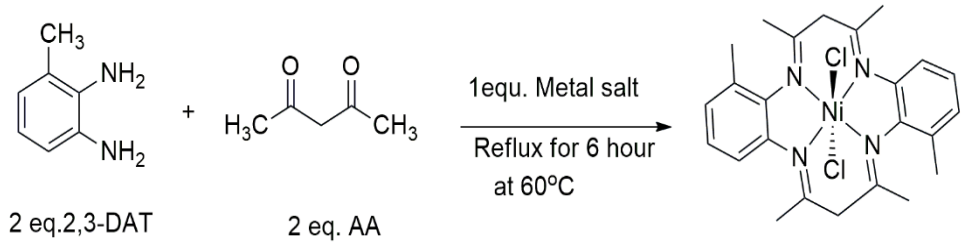

Figure 12. Scheme for the synthesis of Ni complex **31**

The Schiff base ligand, i.e., "4-nitrobenzaldehyde-glycylglycine" (4-NBA-GG, **L32**), and its metal complex with Ni(II) ions (**32**) were successfully prepared (Figure 13) and analyzed by Shiju et al. (2020). These complexes were synthesized using methods that ensured their solubility in water. Spectroscopic analysis indicated that the ligand functions as a tridentate monobasic donor, coordinating via the azomethine nitrogen, carboxylate oxygen, and deprotonated peptide nitrogen atoms. The complexes were confirmed to exhibit octahedral geometry [53].

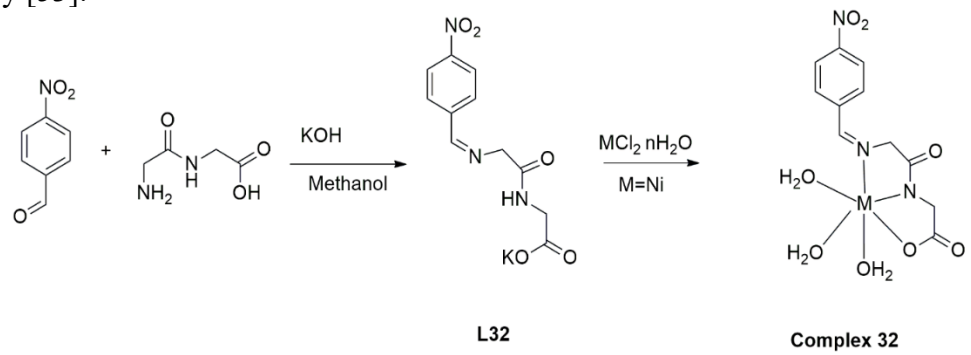

Figure 13. Scheme for the synthesis of Ni complex **32**

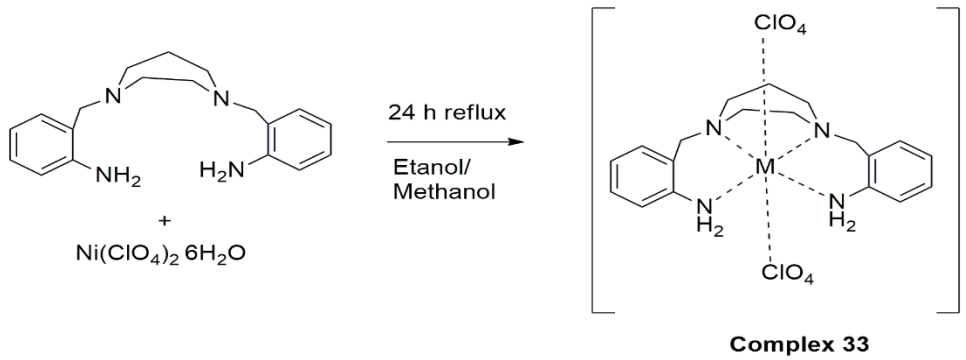

Figure 14. Synthetic scheme of Ni(II) complex **33**

Polyamines (PAs) are organic compounds, either aromatic or aliphatic, characterized by the presence of multiple primary amino groups (–NH_2). These molecules are essential in numerous biochemical processes in humans, animals, and plants [54]. The amino groups in polyamines allow them to serve as donor sites, enabling coordination with metal ions or the

formation of hydrogen bonds with other molecules. These properties make PAs useful in synthesizing both macrocyclic and macrocyclic complexes. The Ni(II) macrocyclic complex (33) was synthesized by reacting 1,4-bis(o-aminobenzyl)-1,4-diazacycloheptane (L33) with the corresponding metal salts (Figure 14) [55].

To prepare MN4 complexes, 3,4-diaminotoluene (2 mmol), acetylacetone (2 mmol), and $NiCl_2 \cdot 6H_2O$ (1 mmol) are dissolved in 50 mL of methanol in a round-bottom flask (Figure 15). The resulting mixture is refluxed for 5-6 hours. Afterward, brown crystals of complex 34, which are collected after re-crystallization [56].

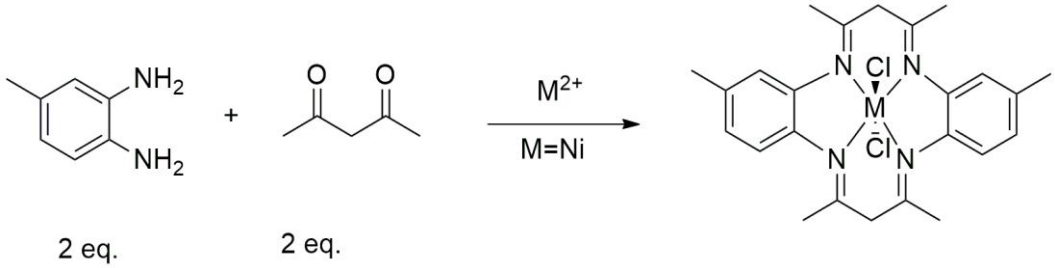

Figure 15. Synthetic scheme of Ni(II) complex **34**

The synthesis of 2,4,9,13,15,20-hexamethyldibenzo-1,4,8,11-tetraazacyclotetra decatetraenec (**L35**) N_4 metal(II) complexes, (**35** & **36,** Figure 16) involves reacting 3,4-diamino toluene (2 mol), acetylacetone (2 mol), and $NiCl_2 \cdot 6H_2O$ in methanol. The reaction mixture is then refluxed at 50 °C for 8 hours. After reflux, the solution is concentrated with a rotary evaporator and placed in a desiccator overnight. The resulting dark brown complexes **35** & **36** are filtered, washed, and recrystallized. Their purity was confirmed by TLC, and they were further characterized using multiple analytical techniques [57].

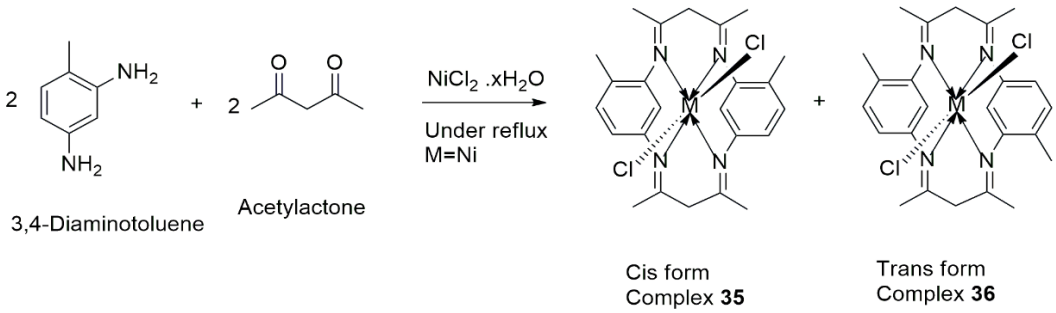

Figure 16. Synthetic scheme of Ni (II) complex **35** and **36**

3. CHARACTERIZATION TECHNIQUES

Elemental analysis, FT-IR, and ^{1}H-NMR spectroscopy were employed to characterize the synthesized metal complexes, confirming their structure and composition.

3.1. FT-IR spectroscopy

The IR spectra of complex **1** showed the disappearance of the ligand's –NH_2 group and the appearance of characteristic bands for the amide –NH and the C=O groups at ~3391 and~1624 cm^{-1}, respectively. Analyzing the IR spectra of a Schiff base ligand (**L1**) and its metal complexes reveals key details about their bonding and coordination sites. The azomethine -CH=N band observed at 1587 cm^{-1} in the free ligand shifts to a lower frequency range (1564–1561 cm^{-1}) in the metal complexes, confirming chelation through the imine nitrogen. This shift suggests a reduction in electron density around the azomethine group due to metal ion coordination. Additionally, changes in the C=O band positions confirm their involvement in bonding with the metal ions. New bands between 641–642 cm^{-1} and 441–446 cm^{-1}, absent in the free ligand, correspond to M-O and M-N vibrations, respectively. Coordinated water molecules in complexes were identified by bands in the 3328–3445 cm^{-1} region, along with symmetric and asymmetric vibrations at 960–968 cm^{-1}, highlighting their role in complex formation [36].

The IR spectra of complex **3** revealed characteristic absorption bands that highlight key structural features. A medium-intensity band observed between 3200-3300 cm^{-1} corresponds to N-H stretching, confirming the presence of amide functionalities in the ligand structure. Peaks in the 1600-1630 cm^{-1} range are ascribed to C=N stretching, further supporting the existence of amidic bonds in the complexes. Moderate-intensity bands between 2820-2950 cm^{-1} arise from =C-H stretching modes. Additionally, bands in the 430-480 cm^{-1} region are associated with M-N stretching, confirming the presence of metal-nitrogen bonds [38].

FT-IR analysis of Schiff base **L11** and its metal complex **11** indicate the presence of azomethine group, initially exhibiting a band at 1610 cm^{-1}, undergoes a shift upon complexation, indicating coordination of its N atom with the metal ion. The phenolic (–OH) group, detected at 3445 cm^{-1} in the free ligand, disappears entirely after complexation, confirming the formation of a metal–oxygen bond. This is further supported by the shift observed in the C–O stretching region and the presence of new absorption bands at 527–533 cm^{-1} and 469–482 cm^{-1}, corresponding to M–O and M–N stretching vibrations, respectively [42].

The FT-IR analysis of the synthesized Ni(II) macrocyclic complex (**22**) displays a characteristic –C=N absorption band in the 1550–1650 cm^{-1} region, confirming the successful condensation of C=O and amino group during macrocyclic complex formation. A lower –C=N vibration frequency suggests electron pair donation from the azo-methine nitrogen to the metal centre. The pyridine ring contributes characteristic bands in the 2343–2415 cm^{-1} region. Additionally, the amide group shows a –C=O stretching vibration between 3450–3720 cm^{-1}. Moderate bands at 2812–2990 cm^{-1} correspond to –C–H stretching of methyl groups, while the 400–480 cm^{-1} range highlights metal-nitrogen (M–N) vibrations, further confirming complex formation [44].

The IR spectral analysis of two macrocyclic metal complexes (**23 & 24)** indicates a prominent band near 1620–1660 cm^{-1}, confirming the C=N group, while the absence of bands around 1700 cm^{-1} and 3450 cm^{-1} indicates the lack of free C=O and NH_2 groups, respectively, supporting successful macrocycle formation. The complexes exhibit characteristic bands around 1100 cm^{-1} and 625 cm^{-1}, signifying the presence of non-coordinated perchlorate groups. Additional peaks at ~1250 cm^{-1}, ~1100 cm^{-1}, ~620 cm^{-1}, and 2950 cm^{-1} are attributed to aromatic and -CH_3 group vibrations. Notably, peaks between 656-625 cm^{-1} suggest substantial interactions between perchlorate groups and the metal cation, though the specific nature of these interactions remains unclear [45].

The IR spectrum of Ni complex **29** displays the disappearance of bands corresponding to free carbonyl (≈1700 cm^{-1}) and amine (≈3200–3400 cm^{-1}) groups. Instead, new bands observed at 1630–1640 cm^{-1} indicated C=N stretching in azomethine and pyridine rings. Bands at 2930–2950 cm^{-1} were assigned to C–H stretching, whereas medium-intensity bands at 1355–1450 cm^{-1} corresponded to aromatic C=C bending vibrations. Additionally, bands in the 420–455 cm^{-1} region confirmed the presence of M–N bonds, signifying reaction between the C=N donor site and the central metal ion [49].

The FT-IR spectral analysis of the Ni complex **31** showed revealed the disappearance of the free carbonyl (>C=O) and amine (–NH_2) bands, which were present in the initial ligands, AA and DAT. Instead, new absorption bands appeared, such as a weak band around 2900 cm^{-1}, attributed to =C–H stretching, and a band at 1497 cm^{-1}, corresponding to asymmetric stretching of the aromatic C=N group. Moreover, a low intensity peak around 3079 cm^{-1} was linked to the aromatic C-H stretching. These spectral features confirm the proposed structures of the N4-metal complexes [52]. The infrared spectrum of complex **33** showed a shift in the NH_2 vibration from 3306–3340 cm^{-1} in the free ligand L33 to 3250–3427 cm^{-1} in complex **33**, indicating coordination to the metal ions. Perchlorate ion absorptions appeared at 1120 and 626 cm^{-1}, unaltered, indicating that they are not directly coordinated to the metal center. New bands in the 415–450 cm^{-1} range were ascribed to metal-nitrogen bonds, confirming metal-ligand coordination [55].

The infrared spectrum of complex **35** lacks a band near 1700 cm^{-1}, confirming the absence of a –C=O group, while the band observed between 1620–1550 cm^{-1} specifies the existence of a –C=N group. Bands observed between 400-480 cm are ascribed to M-N vibrations, confirming the coupling between the metal center and the azomethine nitrogen. Weak absorption bands near 2900 cm^{-1} are allotted to C–H stretching of –CH_3 groups, whereas medium-intensity bands at approximately 1450, 1500, and 1580 cm^{-1} correspond to the bending vibrations of these methyl C–H bonds. Aromatic C=C stretching vibration is observed between 1632–1675 cm^{-1}, and weak bands at 3030–3099 cm^{-1} correspond to Ar–H stretching vibrations. Additionally, the –C=N stretching vibrations are observed between 1580 and 1625 cm^{-1} [56].

3.2. UV-Vis spectral analysis

The UV-Vis spectral analysis of macrocyclic metal complexes reveals important insights into their electronic structure and bonding. Distinct peaks in the spectra confirm alterations in electronic structure upon complexation. Magnetic moment measurements and electronic transitions provide insights into the geometry of the complexes. The Ni complex **1** exhibits bands at 730, 408, and 386 nm with a magnetic moment of 3.16 BM, also indicative of octahedral geometry [36].

UV-Vis spectral analysis for complex **3** in methanolic solutions reveals characteristic absorption bands associated with electronic transitions specific to each metal ion, with NiII complexes showing transitions such as $^{6}A_{1g} \rightarrow {}^{4}A_{1g}$ and $^{6}A_{1g} \rightarrow {}^{4}E_{g}$. Three distinct absorption bands within the ranges of 17,384−18,434 cm^{-1}, 18,719−19,128 cm^{-1}, and 22,565−24,418 cm^{-1}, were also observed. These spectral features suggest a deformed octahedral geometry for the MN_4 complexes. The variation in absorption intensities and positions supports the idea that the coordination environment significantly influences the electronic transitions within these metal complexes [38].

Ni(II) complexes **5–9** showed two distinct absorption bands in their UV-Vis spectra recorded in DMF. The first absorption band, appearing at 338–341 nm, resembled that of the free ligand but with increased intensity, suggesting interaction between the ligand and Ni(II) ion. The second band, observed in the range of 413-418 nm, corresponds to d-d transitions of the Ni(II) ion, highlighting the involvement of the metal in the electronic transitions. These spectral features suggest that the coordination of Ni(II) to the ligands alters the electronic environment, affecting both the ligand and metal complex properties [40].

The synthesized metal complex **11** exhibit a diamagnetic behavior and, based on its electronic spectra and magnetic moment, adopts a square planar geometry. The Schiff base ligand shows characteristic $\pi \rightarrow \pi^*$ and $n \rightarrow \pi^*$ transitions, which shift upon coordination with metal ions, indicating successful complexation. Furthermore, all complexes exhibit a new charge-transfer band, not present in the free ligand, indicating ligand-to-metal interaction. In the visible region, broad d–d transition bands are observed, corresponding to specific electronic transitions unique to each metal ion, such as $1A_{1g} \rightarrow 1A_{2g}$ for Ni(II) [42].

The UV-Vis spectra of macrocyclic metal complexes **23 & 24** in methanol revealed intense absorption bands at 375 and 367 nm attributed to the Schiff base (C=N) chromophore and the $n \rightarrow \pi^*$ transition of phenyl groups attached to carboxylic acids. The Coordination of azomethine nitrogen to the metal centers causes a shift to higher wavelength, observed at 389 nm, likely resulting from a metal-to-ligand charge transfer (MLCT) transition. Additionally, weak absorption bands observed around 600 nm correspond to low-intensity d–d electronic transitions [45].

UV-vis spectra of complex **28** displayed $\pi \rightarrow \pi^*$ transitions in the 200–300 nm range, and distinct electronic transition bands suggested octahedral geometries for the complexes. The

Racah parameter (B) and Nephelauxetic parameter (β) further supported the saddle-shaped octahedral structures for complex **28**. The complex **28** exhibited transitions at 305 nm, 355 nm, and 432 nm. Ligand field parameters, including Dq, B', and β, were determined using Tanabe–Sugano and Orgel diagrams. The Racah parameter (B) was lower for the complexes compared to the free metal ions, while a nephelauxetic parameter ($\beta < 1$) suggested that the metal-ligand bonds possess partial covalent character [49].

The UV-Vis spectra of the metal complex **31** in methanol display peaks at around 255 nm and 280 nm, corresponding to $\pi \rightarrow \pi^*$ and $n \rightarrow \pi^*$ transitions, respectively. The complex shows three peaks at 422 nm, 402 nm, and 392 nm, assigned to the electronic transitions $^3A_{2g}(F) \rightarrow {}^3T_{2g}(F)$, $^3A_{2g}(F) \rightarrow {}^3T_{1g}(F)$, and $^3A_{2g}(F) \rightarrow {}^3T_{1g}(P)$, respectively [52].

The UV-Vis spectrum of complex **34** in methanol (0.001 M) displays three absorption bands at 23,696, 24,875, and 25,512 cm^{-1}, corresponding to the transitions $^3A_{2g}(F) \rightarrow {}^3T_{2g}(F)$ (ε = 5300 L mol^{-1} cm^{-1}), $^3A_{2g}(F) \rightarrow {}^3T_{1g}(F)$ (ε = 4600 L mol^{-1} cm^{-1}), and $^3A_{2g}(F) \rightarrow {}^3T_{1g}(P)$ (ε = 5700 L mol^{-1} cm^{-1}), respectively. Complex **34** displays three absorption bands at 18552, 17605, and 15552 cm^{-1}, corresponding to transitions $^2B_{1g}(G) \rightarrow {}^2B_{2g}(G)$ (ε = 4570 L mol^{-1} cm^{-1}), $^2B_{1g}(G) \rightarrow {}^2E_g(G)$ (ε = 7000 L mol^{-1} cm^{-1}), and $^2B_{1g}(G) \rightarrow {}^2A_{1g}(G)$ (ε = 6400 L mol^{-1} cm^{-1}), respectively [56].

The absorption spectra, highlight key transitions, including $\pi \rightarrow \pi^*$ and $n \rightarrow \pi^*$ transitions, with a strong band around 253 nm and a weaker one around 290 nm. The latter is considered a forbidden transition. The electronic spectrum of Ni(II) complex **35** exhibits bands at 422, 402, and 392 nm, corresponding to specific electronic transitions indicative of an octahedral geometry [57].

Despite extensive drying in both vacuum and in a $CaCl_2$ desiccator, the nickel (II) complex **5** was found to remain in solvated forms. Magnetic susceptibility measurements indicated that complex **5** has an effective magnetic moment of 3.10 μB, calculated from its specific magnetic susceptibility (χr). This magnetic moment is consistent with the expected range for octahedral Ni(II) complexes [40]. The metal complexes **12-21** exhibited a square planar geometry. The Schiff base ligand shows characteristic absorption bands associated with intra-ligand electronic transitions. Additionally, a new absorption band, absent in the ligand, is observed in the complexes, suggesting ligand-to-metal charge transfer. Broad d-d transition bands observed in the visible region confirm the geometry and electronic transitions specific to Ni ion [43].

3.3. Mass spectral analysis

Mass spectral (MS) analysis of the metal complexes offers detailed information about their molecular composition, fragmentation patterns, and confirms the formation of the intended complexes. The MS analysis of the tetraaza perchlorate-coordinated macrocyclic Ni complexes **23** & **24** revealed molecular ion peaks at m/z = 690 for $[C_{24}H_{24}N_4NiCl_2O_{12}]$ and m/z = 573 for $[C_{20}H_{20}N_4NiCl_2O_8]$. The observed peaks correspond to the expected molecular weights,

providing strong evidence in support of the proposed structures of the complexes. This consistency between the mass spectral data and the predicted compositions validates the formation of the reported metal complexes [45].

The molecular ion peaks were observed at m/z 622 for the Ni complex and m/z 625 for the Ni complex **28**, corresponding to the M + 1 fragments. Additional peaks in the range of m/z 600–580, 370–410, and 90–135 likely result from the fragmentation of various structural units within the complexes. These results confirm the composition and structural integrity of the synthesized metal complexes. [49] The mass spectra of both the Ni(II) macrocyclic complex **30** show a distinct fragmentation pattern. The molecular ion peak appears at m/z 401, accompanied by other peaks at m/z 301, 214, 200, and 178, represent the breakdown of the complex [51].

The MS analysis of the NiN_4-complex **31** displayed a molecular ion peak at m/z 501.71, accompanied by fragment peaks at m/z 466, 334, 465, and 431, reflecting its characteristic fragmentation pattern. These results confirm the proposed structures of the metal complexes, validating their expected fragmentation patterns and the presence of key components in both complexes [52].

Mass spectrum indicated the successful formation of the Ni(II) complex **33**, with respective peaks at m/z 570, 575, and 569. The high molar conductivity values (218–244 S cm^2 mol^{-1}) indicate that these complexes behave as electrolytes, likely because of counter ions like perchlorate in solution [55]. The mass spectra of complex **33** displays a molecular ion peak (M+1) at m/z 502, matching the expected molecular weights. Other peaks observed at m/z 487-431, 71 and 490-435, result from the fragmentation of CH and Cl units [56].

In the case of the complex **35**, the mass spectrum recorded in positive ion mode revealed key peaks that suggest the presence of the coordination complex. The most intense peak observed at m/z 431, which represents the base peak, while the molecular ion peak was appeared at m/z 502.2, matching the expected molecular formula. Additional fragments were identified at m/z values of 318, 238, 134, and 71, further confirming the structural breakdown of the complex and supporting the formation of the macrocyclic structure [57].

3.4. Thermogravimetric analysis (TGA)

TGA analysis was carried out to evaluate the thermal stability of the metal complexes, examining mass loss across a temperature range of 25-600°C. The $[Ni(L)Cl_2]$ complex 28 displayed a 10.2% weight loss between 38-78°C, corresponding to the release of moisture, marked by an exothermic peak. Another 6-7% mass reduction occurred between 200-252°C due to the loss of coordinated chlorides, accompanied by a small endothermic peak. At 420°C, a more significant 24% mass loss was detected, attributed to the cleavage of macrocyclic structure, with an endothermic signal. Finally, the complex reached a stable state, indicating the formation of a metal oxide at temperatures up to 600°C [49].

The TGA for complex **35** reveals a weight loss of 8-10% between 40-80°C, owing to the loss of adsorbed solvent molecules, accompanied by an endothermic peak. A further 12% weight loss between 80-300°C, accompanied by a minor exothermic peak, is likely attributed to the loss of axially coordinated chloride ions. Finally, a weight loss of approximately 30% is observed up to 420 °C, accompanied by a sharp exothermic peak, corresponding to the breakdown of the macrocyclic structure [56].

3.5. Elemental analysis and other physical data

Elemental analysis is very important to ensure aligns closely with theoretical values, confirming the proposed compositions. The complex **1** showed good solubility in organic solvents like DMF, acetone, and DMSO but was insoluble in water [36]. Magnetic moments (μeff) indicate paramagnetic behavior for Ni(II). Conductivity measurements for complex **3** suggest non-electrolytic behavior [36]. Elemental analysis for complex **3** supports the proposed compositions, with both complexes exhibiting high yields and melting points near 180–190°C [38]. Elemental analysis for complex 32 revealed a 1:1 metal-to-ligand ratio, indicating a balanced composition between the metal ion and the ligand in these complex **32** [53].

The synthesized complex **11** exhibits square planar geometry at their metal centers. The coordination of ligands around the central metal ion creates a stable configuration, which can impact their reactivity, electronic properties, and potential applications in catalysis or material science. The geometry suggests a preference for planar ligand interactions, typical for Ni ion in such environments [42].

The complex **3** was found to dissolve readily in methanol, DMF, DCM, and acetonitrile, while remaining stable and non-hygroscopic at room temperature. Molecular mass analysis indicates their monomeric structure, while molar conductance studies confirm their non-electrolytic nature [38]. The characterization of the metal complexes **23** & **24** reveals their electrolytic nature with a 1:2 ratio (metal:Ligand), as indicated by their high molar conductance values in MeCN and DMSO. These complexes are stable, hygroscopic, and possess high melting points. They are insoluble in water but dissolve well in MeCN, DMF, and DMSO, producing deeply colored solutions [45].

The Schiff base ligand **L33**, was a yellow-colored compound that is sensitive to air. Due to this sensitivity, the metal complexes with the ligand were synthesized using the template approach. The metal complexes, specifically Ni(II)-4-NBA-GG (**33**), were characterized through various physical and analytical techniques [53].

4. ELECTROCHEMICAL INVESTIGATIONS

The electrochemical behavior of complex **3** was examined under identical conditions in DMSO and DMF solvents (Figure 17). In DMSO, the complex exhibited a quasi-reversible redox process associated with the Ni^{+}/Ni^{2+} pair, characterized by a ΔE value of 0.14 V and a

peak current ratio (ip_a/ip_c) of 1. A cathodic peak was detected at +0.41 V, which corresponds to the reduction process $Ni^{2+} \rightarrow Ni^{+}$. In DMF, the complex showed a similar redox behavior but with reduced peak intensity. Linear relationships between peak current (ip) and the square root of scan rate ($v^{1/2}$) for Ni^{2+}/Ni^{+} redox pairs indicated diffusion-controlled processes, as described by the Randles-Sevcik equation. Diffusion coefficients (D_0) and electron transfer rate constants (K_0) for these processes were calculated using Nicholson and Kochi methods at a scan rate of 100 mV/s.

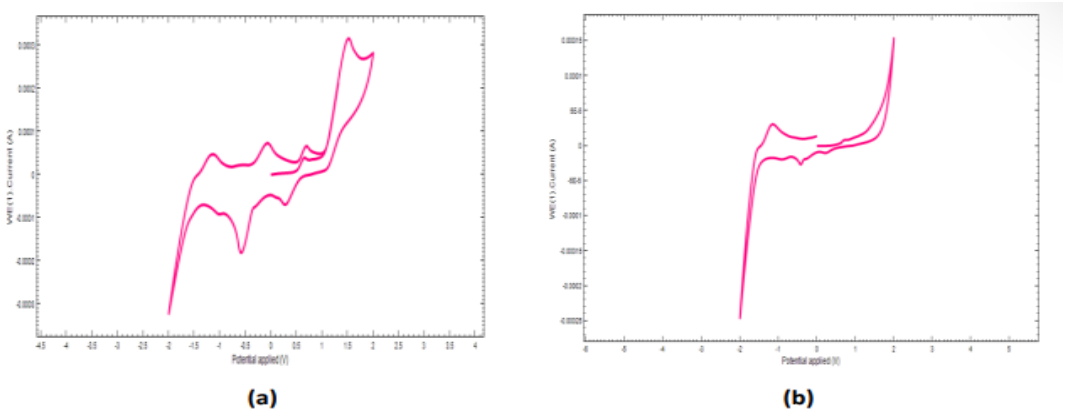

Figure 17. CV plots of Ni^{II} complex in (a) DMSO and (b) DMF with 0.1 M TEAP, recorded at a scan rate of 100 mV s^{-1}. Reproduced from article [38]. Copyright © 2024 by CEE. Reproduction is permitted by the Publishers for non-commercial purposes.

The Ni (II) complex exhibits heterogeneous rate constants of 1.96×10^{-3} cm/s and 1.39×10^{-3} cm/s, respectively in DMSO and DMF. Similarly, diffusion coefficients (D_0) for the Ni(II) complex displays lower values of 2.49×10^{-6} cm^2/s in DMSO and 1.14×10^{-6} cm^2/s in DMF. These observations suggest that the Ni(II) complex 3 has good electron transfer and diffusion dynamics in both solvents [38].

The electrochemical behaviour of the metal complexes was examined through cyclic voltammetry (CV) and rotating disk electrode (RDE) measurements. These studies were conducted on complexes 5-9 utilizing glassy carbon or gold electrodes. The current–voltage curves of both the ligands and Ni(II) complexes were recorded, covering the potential range from zero to the cathodic region for reductions and to the anodic region for oxidations. This allowed for a detailed analysis of the electrochemical characteristics of the metal complexes. The CV curves for Ni(II) complexes 5-9 displayed two irreversible cathodic peaks, indicating the reduction process from Ni(II) to Ni(I) and then to Ni(0) across a potential range of Ep_c = -0.84 to -1.34 V. These peaks were followed by additional reductions in the cathodic region, linked to the reduction of ligand fragments. The Ni(I) and Ni(0) intermediates remained stable on the GC electrode, whereas on the Au electrode, a desorption of the zero-valent Ni(0) metal from the electrode surface was observed following the Ni(I) to Ni(0) reduction. Furthermore, at the Au electrode, desorption peaks were observed on the CVA after ligand oxidation. During

the reverse scan, the reduction peaks shifted to less cathodic potentials, and repeated oxidation led to progressive desorption [40].

The electrochemical behavior of the synthesized metal complex **22** was conducted in DMSO with 0.1 M TEAP as a supporting electrolyte. The CV curves revealed reversible redox systems for both complexes, with [NiL] showing a peak separation of 0.10 V and a formal potential of -1.02 V. The [NiL] complex showed a quasi-reversible Ni^{2+}/Ni^{+} redox couple at +0.32 V, with a peak current ratio near unity [44]. The VC plots demonstrated multiple well-defined redox peaks, suggesting the presence of several electroactive processes with reversible or quasi-reversible behavior. The sharper peaks and stronger current responses indicate higher electrochemical activity in this system.

A typical cyclic voltammogram for Ni complexes 23, 24 is presented in Figure 18. The data revealed a nearly reversible peak for the Ni(II)/Ni(I) redox couple with a ΔEp value of 0.195 V. The $E_{1/2}$ value for this couple was –0.749 V relative to the Ag/AgCl reference electrode. In complex 1, the nickel ion is coordinated with four nitrogen atoms. These nitrogen atoms help stabilize the lower oxidation states, allowing the transition from Ni(II) to Ni(I). A similar pattern was observed in complex 2, with only minor changes in the peak positions [45].

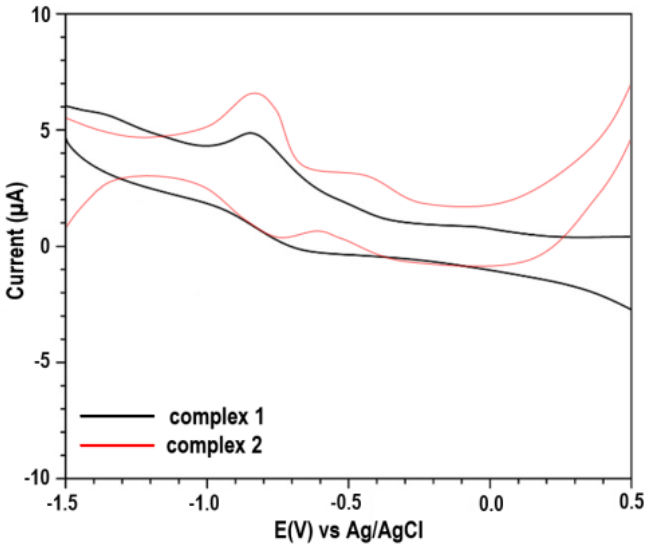

Figure 18. CV plot of complex 23 (black) and complex 24 (red) recorded over a potential range of –1.5 V to +0.5 V versus Ag/AgCl. Both complexes exhibit distinct redox behaviors, with complex 24 showing higher peak currents and more pronounced redox features, indicating greater electrochemical activity compared to complex 23. Adapted from reference [45], Copyright @ The Authors

The CV of the $[NiLCl_2]$ complex 28 displayed a prominent cathodic peak and an anodic peak upon reverse scanning (Figure 19). The observed peak-to-peak separation (ΔE = +0.190 V) and the anodic-to-cathodic peak current ratio (ip_a/ip_c = 0.85) suggest that the redox process

of the complex is quasi-reversible in solution. The wave potential of –0.495 V corresponds to the Ni(II)/(III) redox transition. Additionally, another anodic peak appeared at +0.95 V, suggesting ligand oxidation. Furthermore, CVs of the [Ni(L)Cl_2] complex were recorded at varying scan rates across a potential window of +2 to –2 V. As shown in Figure 19c, the peak current increased with the sweep rate, suggesting rapid electron transfer. However, the ratio of anodic to cathodic peak currents remained nearly constant at varying sweep rates (Figure 19d). An increase in the sweep rate led to a larger peak-to-peak separation between the anodic and cathodic waves, indicating a shift from reversibility to semi-reversibility in the redox process [49].

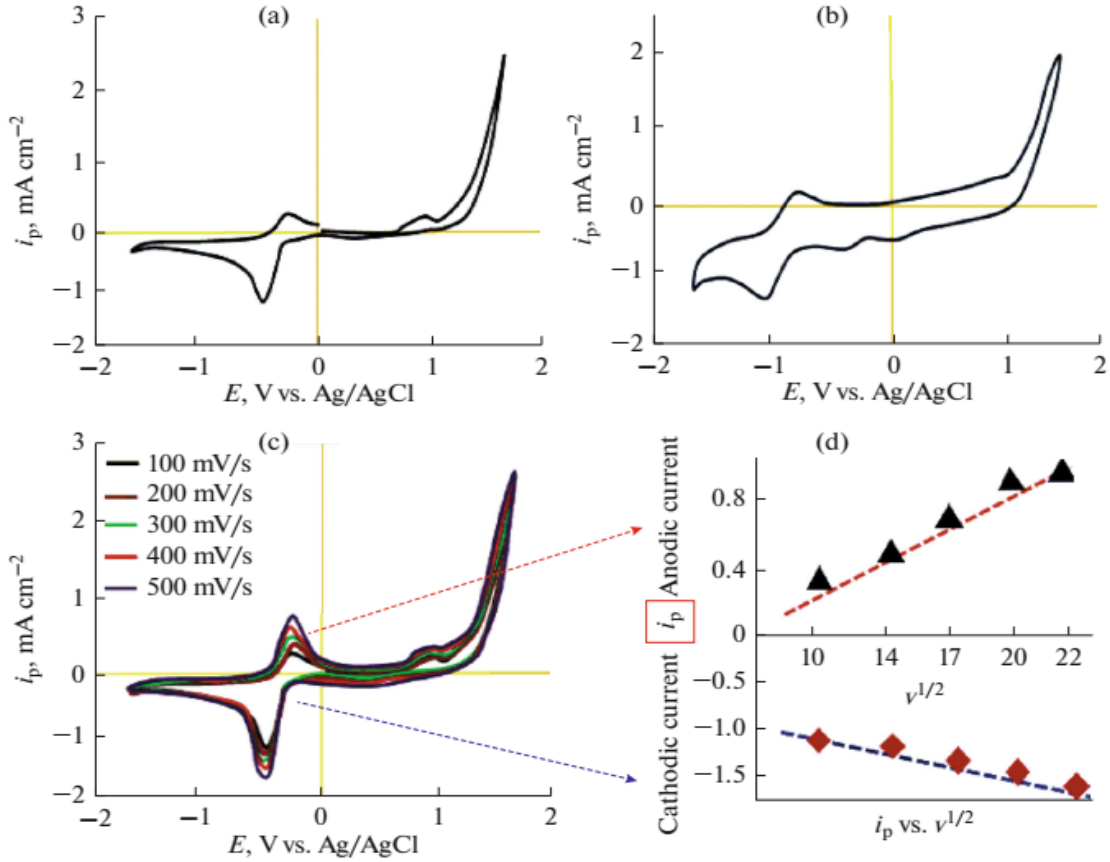

Figure 19. Electrochemical analysis of the synthesized complex. (a) and (b) CV plots of the complex under different experimental conditions, showing distinct redox features and current responses. (c) CV curves recorded at varying scan rates (100–500 mV/s), demonstrating increasing peak currents with scan rate. (d) Linear relationship of anodic and cathodic peak currents (i_p) with the square root of scan rate ($v^{1/2}$), indicating a diffusion-controlled redox process. Adapted with permission from ref. [49].

The electrochemical behavior of the NiN_4-complex 31 was investigated over a potential range of +2 V to –2 V, revealing key insights into their redox properties. The complexes

exhibited reversible redox processes, with NiN_4 exhibited a redox couple at -0.29 V for Ni^{2+} to Ni^{+} conversion and another at -0.68 V linked to ligand redox activity. The substitution of hydrogen atoms with methyl groups in the aromatic and macrocyclic rings enhances the solubility of the complexes in organic solvents. The geometry of these complexes, likely saddle-shaped based on spectroscopic data, influences their electrochemical characteristics. The quasi-reversibility of the redox processes was confirmed by peak separation and an ip_a/ip_c ratio close to unity. Additionally, the linear relationship between ip and $v^{1/2}$, as demonstrated by the Randles-Sevick equation, further supports the electrochemical behavior observed in these complexes [52].

The electrochemical properties of metal complex 34 were examined via cyclic voltammetry in solvents such as MeOH, MeCN, and DMSO, with TEAP serving as the supporting electrolyte. The redox processes observed were distinct. For complex 34, the first redox process (Ni^{2+}/Ni^{+}) exhibited non-Nernstian behavior, with a peak current ratio close to 1, indicating reversibility. The second redox process (Ni^{2+}/Ni^{0}) was Nernstian, occurring at a formal potential of -0.66 V. The CV of complex 34 in MeCN showed similar features to MeOH, though the absence of protons led to changes in the hydrogenation processes of the ligand system [56].

Additionally, there were three distinct cathodic peaks at +0.83 V, -0.19 V, and -0.74 V, linked to Ni-Ni-Ni processes, but these did not align with Nernstian behavior. Controlled potential coulometry of [NiHMTAA]*[2] in MeCN at -0.54 V against Ag/0.1 M AgCl yielded the oxidized [NiHMTAA] species. The oxidation was confirmed by calculating the number of electrons involved ('n' value), which was found to be 0.97, indicating a one-electron transfer. The heterogeneous electron transfer rate constant for these couples was determined, showing that the Ni/Ni redox pair in these macrocycles are stable and resistant to further reduction. This is likely due to the difficulty of the incoming electron being absorbed into the high-energy orbital of the framework [56].

Electrochemical analyses of Me6-tetraaza-[14]-annulenes-type macrocyclic complex 35,36 were performed in DMF. CV was used to examine these complexes within the voltage range of +2 to –2 V. The experiments were performed using 10^{-3} M solutions of the complexes, with 0.1 M TEAP as the supporting electrolyte, under a nitrogen atmosphere [57].

The CV of the complex **35** (Figure 20) shows two redox couples. The first, corresponding to Ni(II)/Ni(III), appears at $E_{1/2}$ = 0.09 V. The second redox couple, corresponding to Ni(0)/Ni(II), involves a two-electron reversible process with an $E_{1/2}$ = 0.05 V. Both redox processes are reversible, exhibiting a peak-to-peak separation (ΔE) of 0.14 V, consistent with the observed peak current ratio. Two distinct cathodic peaks are also observed at Ep_c = +0.62 V and Ep_c = –1.10 V, corresponding to the reductions of Ni(II) to Ni(I) and the ligand (L/L^{-1}), respectively [57].

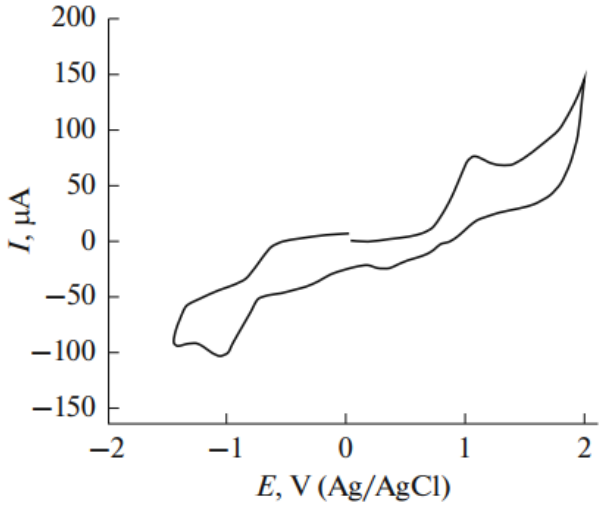

Figure 20. CV plot of complex 35 recorded *vs.* Ag/AgCl; the voltammogram exhibits characteristic redox peaks and a broad anodic wave at positive potentials, indicating the electrochemical behavior and possible oxidation of the Ni(II) center in the complex. Reproduced with permission from reference [57].

In quasi-irreversible redox processes, the observed peak current depends on both charge transfer and mass transfer. The Nernst equation is approximately applicable, and the standard heterogeneous electron transfer rate constant typically falls between 10^{-1} and 10^{-5} cm/s. According to Nicholson's theory, a redox process is deemed reversible when the kinetic parameter (Ψ) exceeds 7, whereas it is considered irreversible if Ψ falls below 0.001. An intermediate Ψ value indicates a quasi-irreversible process [57].

The electroactive species interact with the solvent in a polarization mode, and the choice of solvent significantly influences electron transfer. High-polarity solvents, like DMF, favor electron transfer processes due to their higher dielectric constant. This enhances the diffusion of electroactive species and promotes the adsorption of ion-solvent pairs on the electrode surface, contributing to a higher diffusion coefficient for the electroactive species [57].

5. CONCLUSION

The comprehensive review of Ni(II) macrocyclic and polydentate complexes underscores their pivotal role in advancing both fundamental coordination chemistry and applied sciences, particularly in biological, catalytic, and electrochemical domains. The synthesis strategies, especially the template method, have enabled the rational design of macrocyclic ligands with tailored properties, leading to complexes with enhanced stability, selectivity, and functional versatility. The critical comparison of macrocyclic versus acyclic complexes consistently demonstrates the superior thermodynamic and kinetic stability of the former, attributed to the

macrocyclic effect, which is rooted in the preorganization and entropic advantages conferred by the cyclic ligand framework.

Characterization techniques such as FT-IR, UV-Vis, mass spectrometry, and thermogravimetric analysis have provided robust evidence for the successful formation and structural integrity of these complexes. The spectroscopic data reveal clear shifts in key vibrational and electronic transitions upon metal coordination, confirming the involvement of specific donor atoms and the resulting changes in geometry. The mass spectral and elemental analyses further corroborate the proposed stoichiometries and molecular architectures, while TGA data highlight the remarkable thermal stability of these macrocyclic systems.

Electrochemical investigations have been particularly illuminating, revealing that Ni(II) macrocyclic complexes exhibit diverse and tunable redox behaviors, ranging from reversible to quasi-reversible processes. The redox potentials and electron transfer kinetics are strongly influenced by ligand structure, coordination environment, and solvent polarity. Notably, the stabilization of unusual oxidation states (e.g., Ni(I)) and the facilitation of multi-electron transfer processes position these complexes as promising candidates for applications in catalysis, energy storage, and molecular electronics. The observed diffusion-controlled redox processes and the ability to modulate electron transfer rates through ligand design underscore the potential for fine-tuning these systems for specific technological applications.

Despite these advances, several challenges and knowledge gaps remain. The precise mechanisms underlying the biological activity of these complexes are not fully elucidated, and more systematic studies are needed to correlate structural features with pharmacological outcomes. Additionally, while electrochemical studies provide valuable mechanistic insights, the translation of these findings into practical devices or catalytic systems requires further optimization, particularly with respect to stability, selectivity, and scalability. The environmental impact and potential toxicity of nickel complexes also warrant careful consideration in future applications.

Declarations of interest

The authors declare no conflict of interest in this reported work.

REFERENCES

[1] S. Jimenez-Falcao, and J.M. Mendez-Arriaga, Inorganics 12 (2024) 190.

[2] A.D. Bagul, M. Kumar, A.M. Alanazi, A. Tufail, N. Tufail, D.D. Gaikwad, and A. Dubey, BioMetals 37 (2024) 1713.

[3] V.K. Vashistha, A. Kumar, V.K. Kundi, and D.K. Das, Russ. J. Inorg. Chem. 66 (2021) 61.
[4] M. Claudel, J.V. Schwarte, and K.M. Fromm, Chemistry 2 (2020) 849.
[5] G. Shumi, T. Desalegn, T.B. Demissie, V.P. Ramachandran, and R. Eswaramoorthy, J. Chem. 2022 (2022) 9261683.
[6] V.K. Vashistha, and A. Kumar, Inorg. Chem. Commun. 112 (2020) 107700.
[7] J. Karges, R. W. Stokes, and S. M. Cohen, Trends Chem. 3 (2021) 523.
[8] A. Hu, S. N. MacMillan, and J. J. Wilson, J. Am. Chem. Soc. 142 (2020) 13500.
[9] S.K. Law, Biointerface Res. Appl. Chem. 14 (2024) 64.
[10] A. Kumar, V.K. Vashistha, P. Tevatia, and R. Singh, Anal. Bioanal. Electrochem. 8 (2016) 848.
[11] S. Nasiri Sovari, and F. Zobi, Chemistry 2 (2020) 418.
[12] K. Bajaj, R.M. Buchanan, and C.A. Grapperhaus, J. Inorg. Biochem. 225 (2021) 111620.
[13] Y. Lin, H. Betts, S. Keller, K. Cariou, and G. Gasser, Chem. Soc. Rev. 50 (2021) 10346.
[14] Y.O. Ayipo, W.A. Osunniran, H.F. Babamale, M.O. Ayinde, and M.N. Mordi, Coord. Chem. Rev. 453 (2022) 214317.
[15] J. Liang, D. Sun, Y. Yang, M. Li, H. Li, and L. Chen, Eur. J. Med. Chem. 224 (2021) 113696.
[16] N. W. Kinzel, C. Werlé, and W. Leitner, Angew. Chem. Int. Ed. 60 (2021) 11628.
[17] K. Zou, W. Deng, D.S. Silvester, G. Zou, H. Hou, C.E. Banks, L. Li, J. Hu, and X. Ji, ACS Nano. 18 (2024) 19950.
[18] V. Sharma, V.K. Vashistha, and D.K. Das, Biointerface Res. Appl. Chem. 11 (2020) 7393.
[19] L. Wu, S. Garg, and T.D. Waite, J. Hazard. Mater. 466 (2024) 133526.
[20] A. Soroceanu, and A. Bargan, Crystals 12 (2022) 1436.
[21] A. Kumar, V.K. Vashistha, P. Tevatia, and R. Singh, Spectrochim. Acta A: Mol. Biomol. Spectrosc. 176 (2017) 123.
[22] L.A. Alfonso-Herrera, S. Rosete-Luna, D. Hernández-Romero, J.M. Rivera-Villanueva, J.L. Olivares-Romero, J.A. Cruz-Navarro, A. Soto-Contreras, A. Arenaza-Corona, D. Morales-Morales, and R. Colorado-Peralta, ChemMedChem. 17 (2022) e202200367.
[23] S. Arulmozhi, G. Sasikumar, A. Subramani, M. K. Mohammed, S.J.A. Ali, S. Ponnusamy, M.S. Jabir, A.M. Elgorban, W. Zhang, and H. Natarajan, ACS Omega. 8 (2023) 34458.
[24] V.K. Vashistha, N. Sharma, A. Kumar, and U.R. Sharma, Asian J. Chem. 31 (2019) 2116.
[25] M. S. A. Mansour, A. T. Abdelkarim, A. A. El-Sherif, and W. H. Mahmoud, BMC Chem. 18 (2024) 150.
[26] H. Feizi, F. Shiri, R. Bagheri, J.P. Singh, K.H. Chae, Z. Song, and M.M. Najafpour, Catal. Sci. Technol. 8 (2018) 3954.

[27] Q. Dai, X. Jia, F. Yang, C. Bai, Y. Hu, and X. Zhang, Polymers 8 (2016) 12.
[28] A.F. Orsino, M. Gutiérrez del Campo, M. Lutz, and M.E. Moret, ACS Catal. 9 (2019) 2458.
[29] A. Das, A. Rajeev, S. Bhunia, M. Arunkumar, N. Chari, and M. Sankaralingam, Inorg. Chim. Acta 526 (2021) 120515.
[30] I. Sheikhshoaie, N. Lotfi, J. Sieler, H. Krautscheid, and M. Khaleghi, Transit. Met. Chem. 43 (2018) 555.
[31] H. Arslan, N. Duran, G. Borekci, C. Koray Ozer, and C. Akbay, Molecules 14 (2009) 519.
[32] P. Manimaran, S. Balasubramaniyan, M. Azam, D. Rajadurai, S.I. Al-Resayes, G. Mathubala, A. Manikandan, S. Muthupandi, Z. Tabassum, and I. Khan, Molecules 26 (2021) 823.
[33] A.K. El-Sawaf, F. El-Essawy, A.A. Nassar, and E.S.A. El-Samanody, J. Mol. Struct. 1157 (2018) 381.
[34] N.V. Gerbeleu, V.B. Arion, and J.P. Burgess, John Wiley & Sons (2008) 29.
[35] M. Rezaeivala, and H. Keypour, Coord. Chem. Rev. 280 (2014) 203.
[36] N.A. Mustafa, and S.A. Ahmed, Bull. Chem. Soc. Ethiop. 38 (2024) 1625.
[37] M. Ogawa, S. Usami, R. Takahama, K. Iwamoto, T. Nabeta, S. Kawashima, R. Kojima, J. Ohyama, T. Hayakawa, Y. Nabae, and M. Moriya, Dalton Trans. 53 (2024) 4426.
[38] V.K. Vashistha, D.K. Das, B. Vallamkonda, and S. Yadav, Anal. Bioanal. Electrochem. 16 (2024) 728.
[39] A. Yousri, S. I. Gad, M. A. Abu-Youssef, A. El-Faham, A. Barakat, R. Tatikonda, M. Haukka, and S. M. Soliman, Inorg. Chim. Acta 573 (2024) 122320.
[40] N.I. Vorozhtsov, D.D. Korablina, E.I. Kalenikova, L.A. Sviridova, A.I. Petkova, A.A. Moiseeva, V.A. Tafeenko, A.N. Ataeva, B.V. Makhmudova, A.A. Markova, and A.A. Shtil, Results Chem. 9 (2024) 101632.
[41] J.P. Remiya, B. Shyni, T.S. Sikha, and U.R. Parvathy, J. Coord. Chem. 76 (2023) 729.
[42] K. J. Babu, and D. Ayodhya, Results Chem. 6 (2023) 101110.
[43] B. Wang, D. Sun, S. Wang, M. Chen, H. Liu, Y. Zhou, H. Chen, and Z. Ma, J. Biol. Inorg. Chem. 28 (2023) 627.
[44] Ravinder, D.K. Das, V.K. Vashistha, and A. Kumar, Nano LIFE 12 (2022) 2250007.
[45] V.K. Vashistha, A. Mittal, R. Bala, D.K. Das, and P.P. Singh, Rev. Roum. Chim. 68 (2023) 447.
[46] V. Lozovan, V.C. Kravtsov, I. Bulhac, O. Petuhov, T. Vlase, and P.N. Bourosh, J. Mol. Struct. 1321 (2025) 140021.
[47] V.K. Vashistha, and A. Kumar, Russ. J. Inorg. Chem. 66 (2021) 834.
[48] B. Vinay Kumar, H. C. Ananda Murthy, T. Aravinda, K.N. Harish, and H.S. Bhojya Naik, Nucleos. Nucleot. Nucl. 40 (2021) 896.

[49] V.K. Vashistha, A. Kumar, P. Tevatia, and D.K. Das, Russ. J. Electrochem. 57 (2021) 348.
[50] M. Shebl, A.A. Saleh, S. M. Khalil, M. Dawy, and A.A. Ali, Inorg. Nano-Met. Chem. 51 (2020) 195.
[51] V.K. Vashistha, and A. Kumar, Russ. J. Inorg. Chem. 65 (2020) 2028.
[52] A. Kumar, V.K. Vashistha, S. Ahmed, A. Ali, and D.K. Das, Anal. Bioanal. Electrochem. 12 (2020) 922.
[53] C. Shiju, D. Arish, and S. Kumaresan, J. Mol. Struct. 1221 (2020) 128770.
[54] R. Jastrzab, M.T. Kaczmarek, M. Nowak, A. Trojanowska, and M. Zabiszak, Coord. Chem. Rev. 351 (2017) 32.
[55] H. Keypour, P. Jani, M. Mahmoudabadi, S. Salehzadeh, F. Hajibabaei, S. Faizi, and R. W. Gable, Chem. Pap. 74 (2020) 4433.
[56] V. K. Vashistha, Y. Kumar, A. Kumar, and D.K. Das, J. Sci. Ind. Res. 78 (2019) 788.
[57] V. Sweety, V.K. Vashistha, A. Kumar, and R. Singh, Russ. J. Electrochem. 55 (2019) 161.